Tunable microwave generation of a monolithic dual-wavelength distributed feedback laser

Yen-Hua Lo, Yu-Chang Wu, Shun-Chieh Hsu, Yi-Chia Hwang, Bai-Ci Chen, and Chien-Chung Lin*

Institute of Photonic System, College of Photonics, National Chiao-Tung University, No. 301, Gaofa 3rd Rd, Guiren Dist., Tainan, Taiwan

**chienchunglin@faculty.nctu.edu.tw*

Abstract: The dynamic behavior of a monolithic dual-wavelength distributed feedback laser was fully investigated and mapped. The combination of different driving currents for master and slave lasers can generate a wide range of different operational modes, from single mode, period 1 to chaos. Both the optical and microwave spectrum were recorded and analyzed. The detected single mode signal can continuously cover from 15GHz to 50GHz, limited by photodetector bandwidth. The measured optical four-wave-mixing pattern indicates that a 70GHz signal can be generated by this device. By applying rate equation analysis, the important laser parameters can be extracted from the spectrum. The extracted relaxation resonant frequency is found to be 8.96GHz. With the full operational map at hand, the suitable current combination can be applied to the device for proper applications.

OCIS codes: (350.4010) Microwaves; (140.5960) Semiconductor lasers; (130.0250) Optoelectronics; (130.3120) Integrated optics devices; (060.5625) Radio frequency photonics; (250.5300) Photonic integrated circuits.

References and links

1. G. J. Simonis and K. G. Purchase, "Optical generation, distribution, and control of microwaves using laser heterodyne," IEEE Trans. Microw. Theory Tech. **38**(5), 667–669 (1990).
2. X.-Q. Qi and J.-M. Liu, "Photonic microwave applications of the dynamics of semiconductor lasers," IEEE J. Sel. Top. Quantum Electron. **17**(5), 1198–1211 (2011).
3. J. Yao, "Microwave photonics," J. Lightwave Technol. **27**, 314–335 (2009).
4. D. Marpaung, C. Roeloffzen, R. Heideman, A. Leinse, S. Sales, and J. Capmany, "Integrated microwave photonics," Laser Photon. Rev. **7**(4), 506–538 (2013).
5. A. J. Seeds, "Microwave photonics," IEEE Trans. Microwave Theory Tech. **50**(3), 877–887 (2002).
6. M. J. Fice, E. Rouvalis, F. van Dijk, A. Accard, F. Lelarge, C. C. Renaud, G. Carpintero, and A. J. Seeds, "146-GHz millimeter-wave radio-over-fiber photonic wireless transmission system," Opt. Express **20**(2), 1769–1774 (2012).
7. J.-M. Liu, H.-F. Chen, and S. Tang, "Synchronized chaotic optical communications at high bit rates," IEEE J. Quantum Electron. **38**, 1184–1196 (2002).
8. A. Murakami, K. Kawashima, and K. Atsuki, "Cavity resonance shift and bandwidth enhancement in semiconductor lasers with strong light injection," IEEE J. Quantum Electron. **39**, 1196–1204 (2003).
9. L. Chrostowski, Z. Xiaoxue, and C. J. Chang-Hasnain, "Microwave performance of optically injection-locked VCSELs," IEEE Trans. Microwave Theory Tech. **54**(2), 788–796 (2006).
10. U. Feiste, D. J. As, and A. Ehrhardt, "18 GHz all-optical frequency locking and clock recovery using a self-pulsating two-section DFB-laser," IEEE Photon. Technol. Lett. **6**(1), 106–108 (1994).
11. G. J. Schneider, J. A. Murakowski, C. A. Schuetz, S. Shi, and D. W. Prather, "Radiofrequency signal-generation system with over seven octaves of continuous tuning," Nat. Photon. **7**(2), 118–122 (2013).
12. Y.-S. Juan and F.-Y. Lin, "Photonic generation of broadly tunable microwave signals utilizing a dual-beam optically injected semiconductor laser," IEEE Photon. J. **3**(4), 644–650 (2011).
13. G. E. Villanueva, P. Perez-Millan, J. Palaci, J. L. Cruz, M. V. Andres, and J. Marti, "Dual-wavelength DFB erbium-doped fiber laser with tunable wavelength spacing," IEEE Photon. Technol. Lett. **22**(4), 254–256 (2010).
14. G. E. Villanueva, J. Palací, J. L. Cruz, M. V. Andrés, J. Martí, and P. Pérez-Millán, "High frequency microwave signal generation using dual-wavelength emission of cascaded DFB fiber lasers with wavelength spacing tunability," Opt. Commun. **283**(24), 5165–5168 (2010).

#208831 - $15.00 USD Received 24 Mar 2014; revised 10 May 2014; accepted 11 May 2014; published 22 May 2014

15. B. Sartorius, M. Mohrle, and U. Feiste, "12-64 GHz continuous frequency tuning in self-pulsating 1.55-mm multiquantum-well DFB lasers," IEEE J. Sel. Top. Quantum Electron. **1**(2), 535–538 (1995).
16. X. Wang, W. Mao, M. Al-Mumin, S. Pappert, H. Jin, and L. Guifang, "Optical generation of microwave/millimeter-wave signals using two-section gain-coupled DFB lasers," IEEE Photon. Technol. Lett. **11**(10), 1292–1294 (1999).
17. N. A. Naderi, F. Grillot, K. Yang, J. B. Wright, A. Gin, and L. F. Lester, "Two-color multi-section quantum dot distributed feedback laser," Opt. Express **18**(26), 27028–27035 (2010).
18. J. Huang, C. Sun, B. Xiong, and Y. Luo, "Y-branch integrated dual wavelength laser diode for microwave generation by sideband injection locking," Opt. Express **17**(23), 20727–20734 (2009).
19. C. Laperle, M. Svilans, M. Poirier, and M. Tetu, "Frequency multiplication of microwave signals by sideband optical injection locking using a monolithic dual-wavelength DFB laser device," IEEE Trans. Microwave Theory Tech. **47**(7), 1219–1224 (1999).
20. N. Kim, S.-P. Han, H.-C. Ryu, H. Ko, J.-W. Park, D. Lee, M. Y. Jeon, and K. H. Park, "Distributed feedback laser diode integrated with distributed Bragg reflector for continuous-wave terahertz generation," Opt. Express **20**(16), 17496–17502 (2012).
21. N. Kim, J. Shin, E. Sim, C. W. Lee, D.-S. Yee, M. Y. Jeon, Y. Jang, and K. H. Park, "Monolithic dual-mode distributed feedback semiconductor laser for tunable continuous-wave terahertz generation," Opt. Express **17**(16), 13851–13859 (2009).
22. G. Carpintero, K. Balakier, Z. Yang, R. C. Guzman, A. Corradi, A. Jimenez, G. Kervella, M. J. Fice, M. Lamponi, M. Chtioui, F. van Dijk, C. C. Renaud, A. Wonfor, E. A. J. M. Bente, R. V. Penty, I. H. White, and A. J. Seeds, "Photonic integrated circuits for millimeter-wave wireless communications," J. Lightwave Technol. (2014).
23. M. Zanola, M. J. Strain, G. Giuliani, and M. Sorel, "Monolithically integrated DFB lasers for tunable and narrow linewidth millimeter-wave generation," IEEE J. Sel. Top. Quantum Electron. **19**(4), 1500406 (2013).
24. D. Liu, C. Sun, B. Xiong, and Y. Luo, "Suppression of chaos in integrated twin DFB lasers for millimeter-wave generation," Opt. Express **21**(2), 2444–2451 (2013).
25. C. Zhang, S. Liang, H. Zhu, and W. Wang, "Widely tunable dual-mode distributed feedback laser fabricated by selective area growth technology integrated with Ti heaters," Opt. Lett. **38**(16), 3050–3053 (2013).
26. M. Soldo, N. Gibbons, and G. Giuliani, "Narrow linewidth mm-wave signal generation based on two phase-locked DFB lasers mutually coupled via four wave mixing," in *Conference on Lasers and Electro-Optics/International Quantum Electronics Conference* (Optical Society of America, Baltimore, Maryland, 2009), p. JThE32.
27. C.-Y. Chien, Y.-H. Lo, Y.-C. Wu, S.-C. Hsu, H.-R. Tseng, and C.-C. Lin, "Compact photonic integrated chip for tunable microwave generation," IEEE Photon. Technol. Lett. **26**(5), 490–493 (2014).
28. K. Inoue, T. Mukai, and T. Saitoh, "Nearly degenerate four-wave mixing in a traveling-wave semiconductor laser amplifier," Appl. Phys. Lett. **51**(14), 1051–1053 (1987).
29. C.-C. Lin, C.-Y. Chien, Y.-C. Wu, H.-C. Kuo, and C.-T. Lin, "Evaluation of tunable microwave signals generated by monolithic two-section distributed feedback lasers," in *CLEO: 2013* (Optical Society of America, San Jose, California, 2013), p. JTh2A.104.
30. J.-M. Liu and T. B. Simpson, "Four-wave mixing and optical modulation in a semiconductor laser," IEEE J. Quantum Electron. **30**(4), 957–965 (1994).
31. I. Petitbon, P. Gallion, G. Debarge, and C. Chabran, "Locking bandwidth and relaxation oscillations of an injection-locked semiconductor laser," IEEE J. Quantum Electron. **24**, 148–154 (1988).
32. F. Mogensen, H. Olesen, and G. Jacobsen, "Locking conditions and stability properties for a semiconductor laser with external light injection," IEEE J. Quantum Electron. **21**, 784–793 (1985).
33. A. Hurtado, J. Mee, M. Nami, I. D. Henning, M. J. Adams, and L. F. Lester, "Tunable microwave signal generator with an optically-injected 1310 nm QD-DFB laser," Opt. Express **21**(9), 10772–10778 (2013).
34. C.-C. Lin, G. Yoffe, M. Emanuel, S. Rishton, D. Ton, S. Zou, B. Lu, and B. Pezeshki, "Monolithically integrated high speed DFB BH laser arrays for 10Gbbased LX4 application," in *Optical Fiber Communication Conference and Exposition and The National Fiber Optic Engineers Conference* (Optical Society of America, Anaheim, California, 2006), p. OWI84.
35. T. B. Simpson, J. M. Liu, A. Gavrielides, V. Kovanis, and P. M. Alsing, "Period-doubling cascades and chaos in a semiconductor laser with optical injection," Phys. Rev. A **51**(5), 4181–4185 (1995).
36. Y. Kotaki, S. Ogita, M. Matsuda, Y. Kuwahara, and H. Ishikawa, "Tunable, narrow-linewidth and high-power lambda /4-shifted DFB laser," Electron. Lett. **25**(15), 990–992 (1989).
37. B. Dahmani, L. Hollberg, and R. Drullinger, "Frequency stabilization of semiconductor lasers by resonant optical feedback," Opt. Lett. **12**(11), 876–878 (1987).
38. K. Petermann, "External optical feedback phenomena in semiconductor lasers," IEEE J. Sel. Top. Quantum Electron. **1**(2), 480–489 (1995).
39. H.-K. Sung, E. K. Lau, and M. C. Wu, "Optical single sideband modulation using strong optical injection-locked semiconductor lasers," IEEE Photon. Technol. Lett. **19**(13), 1005–1007 (2007).
40. P. Gallion, G. Debarge, and C. Chabran, "Output spectrum of an unlocked optically driven semiconductor laser," Opt. Lett. **11**(5), 294–296 (1986).
41. J. Sacher, D. Baums, P. Panknin, W. Elsässer, and E. O. Göbel, "Intensity instabilities of semiconductor lasers under current modulation, external light injection, and delayed feedback," Phys. Rev. A **45**(3), 1893–1905 (1992).
42. V. Kovanis, A. Gavrielides, T. B. Simpson, and J. M. Liu, "Instabilities and chaos in optically injected semiconductor lasers," Appl. Phys. Lett. **67**(19), 2780–2782 (1995).

#208831 - $15.00 USD Received 24 Mar 2014; revised 10 May 2014; accepted 11 May 2014; published 22 May 2014

43. S.-C. Chan, S.-K. Hwang, and J.-M. Liu, "Period-one oscillation for photonic microwave transmission using an optically injected semiconductor laser," Opt. Express **15**(22), 14921–14935 (2007).
44. T. B. Simpson and J. M. Liu, "Phase and amplitude characteristics of nearly degenerate four-wave mixing in Fabry–Perot semiconductor lasers," J. Appl. Phys. **73**(5), 2587–2589 (1993).

1. Introduction

Since its invention in 60 years ago, the semiconductor laser has become an integral part of our daily lives. One of its important applications is microwave photonics (MWP) [1–5] which combines the merits from the radio-frequency engineering and optoelectronic devices. Many MWP researches in which the semiconductor lasers were heavily involved have been published: broadband wireless access network [4, 6], chaotic wave generation [7], resonant frequency enhancement [8, 9] and all optical clock recovery [10] etc. The roles of semiconductor lasers in these experiments were usually the sources of microwave signals via mechanisms such as optical heterodyne, self-pulsation, or external modulation [4]. In these mechanisms, optical heterodyne which mixes two different wavelengths of photons to generate the differential microwave frequency is the most popular choice due to its simplicity. Discrete laser modules (tunable or non-tunable) were first applied in the system level to utilize this effect [1, 11, 12]. In these schemes, large system setup and various independent optical components were necessary to achieve the required performance. Other methods such as integrated erbium doped fiber gratings to achieve the dual-wavelength operation and the microwave generation were also proposed and demonstrated [13, 14]. As the optoelectronic devices quickly evolved into integrated circuit scale, so did the MWP related devices. The microwave generation of a two-section distributed feedback laser was first proposed and demonstrated in the 1990s [10, 15–17]. Meanwhile the Y-branch design to combine two lasers also showed great progress [6, 18, 19]. In recent years, more sophisticated photonic integrated circuitry (PIC) has been applied to the microwave generation as well [20–26]. Compared to Y-branch or the PIC design, the two-section (or multiple-section) lasers are much easier to fabricate without extra epitaxial regrowth which can reduce the device yield. However, the in-line architecture of the two-section lasers inherently has optical fields of lasers strongly interfering with each other, and thus increases the complexity of the microwave operation. Many two-section devices relied on either strong grating strength or gain-coupled grating to obtain suitable microwave signals [10, 15, 16].

Previously, we reported a design to incorporate nano-scale distributed Bragg reflector (DBR) into the two-section DFB lasers to achieve continuous frequency tuning of microwave signals up to 25GHz [27]. In our prior work, most of the microwave signals were generated due to the four-wave mixing effect caused by nonlinear refractive index change in the laser gain medium [28]. In this paper, a detailed investigation on the operation of such devices is performed. The combination of different driving currents was fully tested and corresponding optical and microwave behaviors are analyzed. Different regimes of operations can be mapped and we could identify suitable driving currents for different applications.

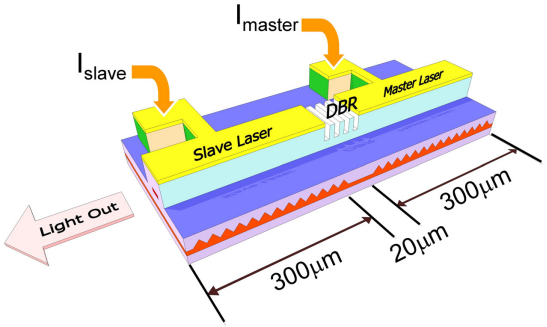

Fig. 1. The schematic diagram of a monolithic two-section DBR DFB laser.

#208831 - $15.00 USD Received 24 Mar 2014; revised 10 May 2014; accepted 11 May 2014; published 22 May 2014

2. Device fabrication

The device was grown on a n-type InP substrate by metalorganic chemical vapour deposition (MOCVD) technique. A grating designed for 1550nm was first patterned by E-beam lithography. The active region is formed by multiple InGaAsP quantum wells. Mesa-etch and subsequent epitaxial re-growth were performed to create the buried heterostructure. The wafer was then underwent regular semiconductor processes to construct the ridge waveguide and p-type electrical contacts. The finished sample was thinned down for n-type backside contact and bar/chip cleaving and suitable ceramic submounts were used for die-attachment. The detailed device fabrication was described previously [27, 29].

After the regular semiconductor processes, the final stage of the fabrication is the nano-scale focused ion beam (FIB) etch to form the DBR section. This step was done by a FEI Nova 200 system equipped with the 30 keV Ga atom as the etching source. The chamber pressure is around 7.5×10^{-6} torr. The etch rate was controlled by the monitoring current and tuned to be around 0.3 μm/min.

One of the important components in this integrated chip is the DBR structure. The role of the DBR section in our chip is three-fold: the first is to provide an electrical isolation between two lasers via cutting through the p-type layer; the second is to provide a highly-reflective facet which can ensure the single mode operation in a DFB laser; and the third is to provide suitable optical coupling into the other laser. The air gap and semiconductor arrangement can provide a dramatic change of refractive index, which can reflect the photons very efficiently. Therefore, high reflectivity can be expected from very few pairs of DBR. From the calculation combined with effective index method and transmission matrix, a 99.97% reflectivity can be achieved by 3.5 pairs of DBR. However, the devices with 3.5 or fewer pairs of DBR tend to be multi-mode and the actual measurements of the injected intensities among 4.5 or more pairs of DBR structures stay almost the same and this phenomenon indicates that the reflectivity saturates after 4.5 pairs. The central wavelength of the DBR is the same with the DFB gratings (1550nm) and since the bandwidth of such structure is very wide (about 100nm or more), a 10% departure from the designated wavelength will not hurt the device [27].

On the completed device, as shown in Fig. 1, two DFB lasers are separated by a DBR section which plays the role of both mirror and optical coupler. The deep air trench (around 5 to 6 μm) of DBR section ensures the electrical isolation. The cavity length of the DFB laser is 300 μm while the DBR section is 20 μm. To obtain high reflectivity for individual DFB lasers, 6.5 pairs of air/semiconductor DBR structure were etched. The DBR is designed with $3/4\lambda$(= 1162nm) for air trench width and $5/4\lambda$(= 584nm) for semiconductor width, and the designated wavelength (λ) is 1550nm. When all the processes are finished, the facet on the DBR side has a high reflectance, and the other uncoated facet has a much lower, native Fresnel reflectance of air/InP. Such asymmetric reflecting powers between two facets of individual DFB lasers can produce a single longitudinal mode operation across most of the driving currents with much greater yield.

#208831 - $15.00 USD Received 24 Mar 2014; revised 10 May 2014; accepted 11 May 2014; published 22 May 2014

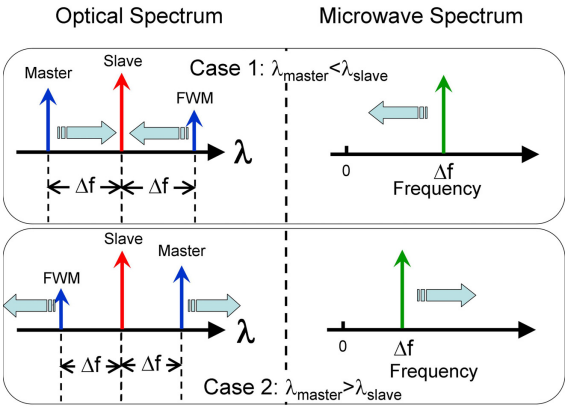

Fig. 2. The simplified operational principle of a two-section single mode laser for microwave generation in the optical heterodyne. The corresponding microwave spectrum is listed side by side with its optical counterpart.

3. Operational principle

From Fig. 1, we denote the DFB laser at the output facet as the slave laser and the other one as the master laser. Traditionally, the master laser provides the injection signal while the slave laser receives this injection power. This nomenclature comes from the injection locking scheme where the slave laser is controlled by the injection of the master laser. However, due to the monolithic nature of this chip, these two lasers are mutually coupled, i.e. the light from one laser can inject into the other one and vice versa, such that the names (slave and master lasers) are just for the purpose to distinguish between the output side (slave) and backside (master) components of the chip, and the output signal is always taken from the front facet of the slave laser. When two monochromatic photons meet in the resonant cavity of the slave laser, many scenarios could happen. One of them is the weakly injection case in which the two wavelengths of photons co-exist in the same cavity and the carrier modulation due to this mixed optical field induces the refractive index changes, and a resulting four-wave-mixing output can be expected [28, 30]. When this mixed optical signal hits the high-speed photodetector, the resultant electrical output will be in the differential frequency of the two colors of photons, called detuning frequency Δf, and can be written as:

$$\Delta f = c\left(1/\lambda_{master} - 1/\lambda_{slave} \right), \tag{1}$$

where c is the speed of light, λ_{master} and λ_{slave} are the emission wavelengths of the master and slave lasers, respectively.

Figure 2 shows the simplified operational principle of our devices. When a DFB laser operated above its threshold, one specific driving current to the laser corresponds to one emission wavelength. In our integrated chip, two cases can be discussed here: the first one is when the master laser emission peak is on the shorter wavelength side. The current of the slave laser (I_{slave}) is kept the same and we turn up the current of the master laser (I_{master}) to make its emission peak approach the slave laser's. On the optical spectrum, the FWM peak rises due to the four-wave-mixing effect mentioned earlier, and it locates at the same detuning frequency Δf from the slave lasers peak but on the other side. As the I_{master} keeps increasing, the peak wavelength of the master laser red-shifts and the Δf reduces until the master laser emission peak coincides with the slave laser's. From the microwave spectrum, the differential frequency Δf can be seen moving towards zero as the I_{master} increases. In the second case, the emission peak of the master laser is on the longer wavelength side and moves away from the slave laser's. This situation will produce a similar FWM peak in the optical domain and the signal in the

#208831 - $15.00 USD Received 24 Mar 2014; revised 10 May 2014; accepted 11 May 2014; published 22 May 2014

microwave spectrum. However, when I_{master} goes up, the gap between the two laser's peak keeps growing and so does the FWM signal. On the microwave spectrum, the RF signal now moves towards the high frequency from the zero point until the detection limit or the FWM effect diminished.

Depending on the wavelengths at low driving currents, we could have both cases on the same device or just one of them. The former situation is useful for laser dynamic analysis since both positive and negative Δf can be produced, while the latter condition might be preferable for microwave carrier generation because of the extended Δf range at the same current span.

In any cases, the combination of different driving currents of the two lasers represents possibilities of different generated microwave signal, and with this feature, a wide-range electrically tunable microwave source can be realized.

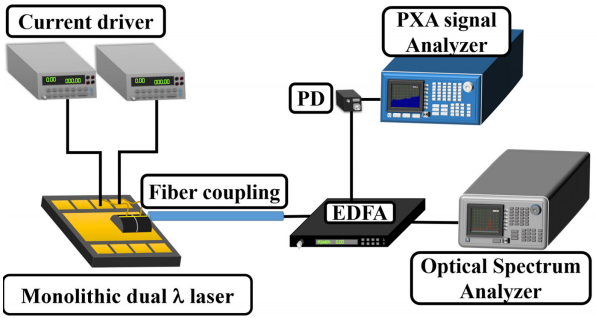

Fig. 3. Measurement setup for both microwave and optical spectrum. Suitable in-line isolators were used in the connecting optical fibers to prevent from back scattering.

4. Device characterization

The individual device characteristics was first tested by a DC current driver and a broadband photodetector. A threshold current of 6 to 10mA was found in most of devices. Devices with side mode suppression ratio (SMSR) better than 40dB can also be selected from different sections of wafers. The purity of the optical mode in the laser is essential for the device to work in the microwave generation. Both electrical and optical characteristics are similar to the devices presented before [29]. To test the two-section lasers in action, a three- probe station is necessary and we use an angled-cleaved fiber for efficient light coupling. An erbium-doped fiber amplifier (EDFA) is used for boosting the overall optical signal before it enters an 1 by 2 splitter.

After the splitter, the photons are fed into either optical spectrum analyzer or a u2t 50GHz photodetector (PD). The output of the highspeed PD is fed into an Agilent N9030A PXA signal analyzer for RF spectrum. The whole setup is illustrated in Fig. 3.

The complete measurements of the integrated lasers include the optical and microwave spectrum. With the weakly injection stemming from the high reflectivity of DBR section, the locking between the master and slave laser is not strong, and the locking range is limited [8, 31, 32]. However, outside of this injection locked zone, a wide range of FWM operation can be expected [8, 12, 33].

#208831 - $15.00 USD Received 24 Mar 2014; revised 10 May 2014; accepted 11 May 2014; published 22 May 2014

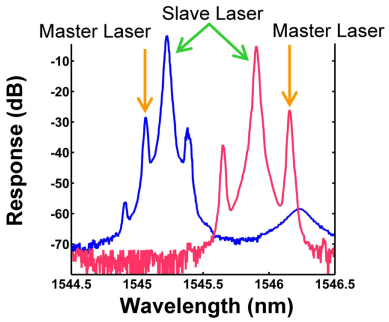

Fig. 4. The combined optical spectrum from the output facet of the slave laser, under different conditions: I_{slave} = 50mA, I_{master} = 16mA (blue), and I_{slave} = 50mA, I_{master} = 72mA (red). The corresponding emission peaks of the slave and master lasers are marked for clarity.

For the optical spectrum, a typical four-wave-mixing pattern, as shown in Fig. 4, can be observed across a wide range of pumping currents. Depending on the relative location of emission wavelengths between the slave and master laser, both cases shown in Fig. 2 are found in our devices. One typical situation in Fig. 4 is that the emission wavelength of the master laser at the low driving current is shorter than the slave laser's, and it sweeps across the slave laser's peak as we increase the driving current of the master laser. In this condition, both positive and negative detuning frequency (Δf) can be found. The slave laser's peak red-shifts slightly due to the rising temperature brought by the increased I_{master}, but this red-shifting rate is slower than the master laser's such that the master laser's peak catches up eventually. We could visualize these variations by putting all of the optical spectrum under different I_{master} together in a contour plot in Fig. 5. In this figure, the slave laser is constantly driven at 50mA while the current of the master laser varies from 16mA to 80mA. The peak of the master laser moves much faster (dash-dot line) and catches up with the slave laser's (white dash line). A notch of the slave laser's trace is observed around I_{master} = 38mA, indicating a possible injection locking of this device, in which the slave laser's emission peak is pulled to the master laser's. But this injection locking range is narrow in our case, so the two peaks deviate from each other shortly after I_{master} = 40mA. The separation between the slave and master laser's emission produces the signal at difference frequency according to Eq. (1) and can be explained in the following paragraph.

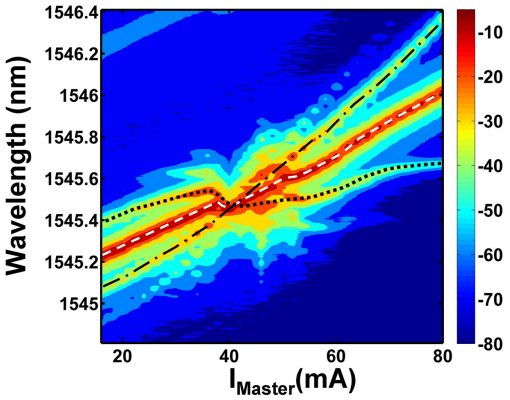

Fig. 5. The collection of optical spectrum of the two-section DFB lasers at I_{slave} = 50mA and various I_{master}. The color bar represents the relative intensity measured in dBm, and the white dash line marks the trace of the emission peak of the slave laser. The dash-dot line is from the peak of the master laser and the dot line is the FWM signal.

#208831 - $15.00 USD Received 24 Mar 2014; revised 10 May 2014; accepted 11 May 2014; published 22 May 2014

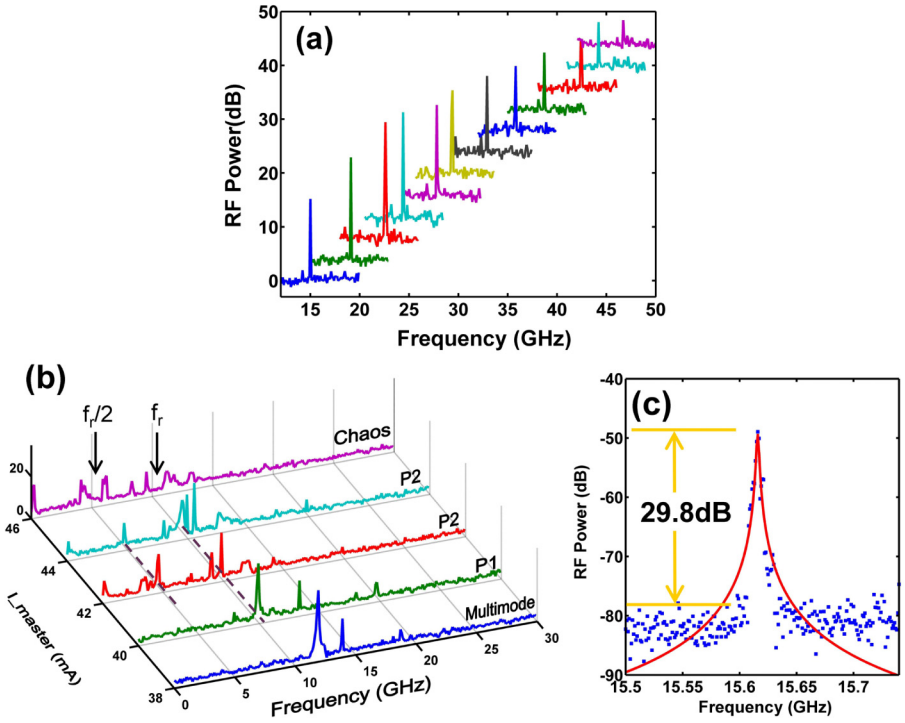

Fig. 6. (a)The single mode microwave spectrum read by Agilent N9030A showing the continuous tuning. (b) The development of different states from multi-mode to chaos under different master currents. (c)The detailed single mode spectrum. The blue dots are measured data and the red curve is the fitted Lorentzian function.

Other than optical spectrum, the RF electrical spectrum of the device was also taken. The output photocurrent of the highspeed PD in Fig. 3 can carry the beat signal of the two lasers' photons. As mentioned in the previous section, this beat note can be tuned by changing the driving current of the lasers. Figure 6(a) shows a series of single-mode RF spectrum at various combinations of I_{master} and I_{slave}. When the slave laser's current is fixed and the master laser's is changing, different dynamic behaviors can be observed. The RF signal starts with single mode when the wavelengths of the two lasers are far apart, and evolve into multiple mode, period-one (P1) state, period-two (P2) state, and chaos mode when the wavelengths are getting closer as we increase the I_{master}. In Fig. 6(b), the gradual development of the RF signals under different master laser current is demonstrated. At I_master = 38mA, the RF signal shows a multimode spectrum. Then at 40mA of master current, the strong peak at relaxation resonant frequency (f_r is around 10 GHz by the measurement for this type of device [34]) indicates the device entering P1 state [35]. As the I_master keeps increasing, a second peak at 5GHz can be seen at 42 and 44mA, and the device enters the P2 state [35]. Once the current increases to 46mA, the RF spectrum shows the pattern with broad-band, multiple peaks, and the disappearance of the signatures of f_r and $f_r/2$ peaks, suggesting the device is in chaotic condition [35]. When I_{master} is further increased, the two lasers will be untangled again and the single mode spectrum can be expected. Even though the electrical spectrum is spiky during the locked or chaos condition, the actual coverage of the single mode operation is still wide according to our complete mapping. Linewidth of single mode signal is acquired by fitting the data with the Lorentzian function, and a value of 2.22MHz is extracted. This full-width at half maximum is close to what we reported before (1.99MHz) [29] based on the same type of device and this variation could result from the differences between devices. From Fig. 6(b), a side mode suppression ratio of 29.8dB can be obtained. This linewidth stems from the convolution of the two lineshapes of the lasers,

#208831 - $15.00 USD Received 24 Mar 2014; revised 10 May 2014; accepted 11 May 2014; published 22 May 2014

and thus becomes the summation of the linewidths of the two lasers. To further reduce this linewidth to kHz regime, a longer resonant cavity with weak DFB grating strength can be a good solution [36]. Other choice will be using an extra optical feedback mechanism to crop the linewidth to 10kHz or below [37, 38]. Another method is to modulate one of the lasers to have side-band injection-locking achieved [39]. However, due to the mutual-injection nature of our device, this effect might be complicated, and need to be seriously analyzed first. On the measurement setup side, improvements of current stability and precise temperature control can also reduce the frequency noise and thus the linewidth.

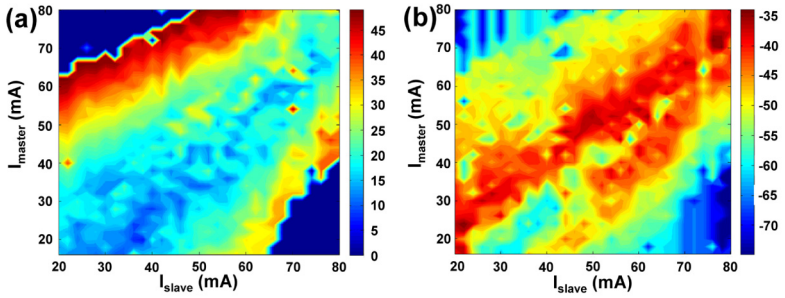

Fig. 7. (a) The measured peak frequencies (in GHz); (b) max RF power (in dBm) under different driving currents of the slave and master lasers. The colors of the contour plots indicate the corresponding intensities showing in the color bar.

5. RF dynamic behavior mapping at different current combination

As we could see from the previous section, the resultant RF signals from the dual-wavelength DFB laser can be very complex and a thorough investigation on all the possible patterns will be necessary for engineering purposes. Previously, the RF dynamic behavior of an optically injection-locked laser was carefully studied with independently-driven, discrete components [30, 40, 41]. Under this circumstance, the injection power and the separation of emission wavelength can be willingly changed to explore different regimes of operations. However, in an integrated chip, this is not easy to implement, and we have to examine the problem at a different angle: from the current combination of the master and slave lasers. These are the knobs that can be tuned during the experiments. By different driving currents of master and slave lasers, both the external injected power and the emission wavelength are varied, and their combined optical and microwave spectrum are recorded. The testing grid was made by a 33 × 33 matrix of current combination sweeping from 16mA to 80mA with a 2mA increment on each laser. Figure 7 shows both the peak RF frequency and its peak power intensity in dBm. From the plots, a sharp change occurs at both high I_{slave} /low I_{master} and low I_{slave} /high I_{master} cases due to the limitation on the PD frequency response (up to 50GHz at most).

As shown in previous section, comparison between the RF and optical spectrum at the same current level can reveal the type of dynamic behaviors in the slave laser. Single and multiple peaks can be found at high- frequency cases when the injection is weak and the slave laser is in FWM state. When two laser's emission peaks are close to each other, injection locking, P1, P2, and chaos can be expected [42]. To distinguish among these different modes (multi-mode, P1, P2, chaos), the frequency of the main peak is very important. Between zero and relaxation resonant frequency (f_r), the RF signal can be categorized as in P1 or P2 or chaotic state. Once the main peak frequency goes beyond f_r, only single or multi-mode will be recorded for the signal pattern because the two lasers' wavelengths are now far apart. Within the f_r range, the P1 state can be detected by a strong single peak at f_r and this peak usually does not change its location even when the driving current is slightly changed. The P2 state can also be easily identified when there are at least two main peaks appearing at f_r and $f_r/2$ [35]. When the RF signal starts evolving into multiple peaks and broad-band pattern, then we could suggest the

#208831 - $15.00 USD Received 24 Mar 2014; revised 10 May 2014; accepted 11 May 2014; published 22 May 2014

device is now into the chaotic mode. By using these criteria, we could build the dynamic behavior map shown in Fig. 8. In the diagonal direction of Fig. 8, where the two lasers have similar emission wavelengths, more vibrant changes of the operations are observed, and the chaotic pattern takes a large portion.

Needless to say, the random peaks in the RF spectrum due to chaos are not welcomed in microwave carrier generation. However, the P1 mode, in which a more stable peak at resonant frequency (f_r) is generated, is possible for optical clock recovery. The most anticipated behavior should still be the single mode operation which can be useful for many applications. Between Fig. 7 and Fig. 8, the range of single mode and their output RF powers can be mapped directly. A continuous distribution of single mode operation is possible from 15GHz all the way to 50GHz. Although the PD cannot detect the signal beyond 50GHz, we could calculate the largest wavelength separation (thus the RF frequency) with FWM effect on the optical spectrum, and the value come up with 70GHz. With Fig. 8 available, any engineer can pick up the right combination of the I_{slave} and I_{master} to generate the desired RF signals in terms of frequencies and powers.

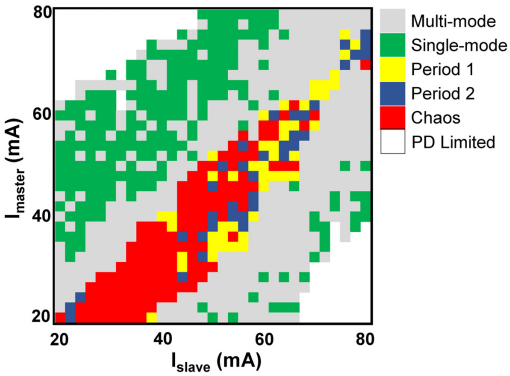

Fig. 8. The dynamic behavior map of the two-section laser at the same current combination as in Fig. 7. The colors represent the mode of operation judged by RF and optical spectrum.

The finished map is definitely very different from what was shown before [42, 43]. The main reason is because different variables, i.e. the laser driving currents, are used to record this map. Our chip is monolithically integrated such that it is not possible to independently tune the injected power and detuning frequencies. On our chip, the wavelength always move to longer side as the driving increases and the injected power also increases with the same direction. So at some current combinations, the same detuning frequency and the injected to free-running power ratio is repeated inevitably, which will in turns make our map look differently. Another constraint in our map is the precision of our current source. Every mA up or down means a 2.5GHz change in our lasers. So any fine structures shown in previously-reported dynamic maps could be bypassed due to this reason.

6. Laser parameter extraction

When the slave laser is in FWM state, valuable laser parameters can be extracted from the optical and microwave measurement [28, 30, 43, 44], and the related formula have been developed long time ago. From the optical spectrum, three distinctive peaks can usually be identified: main, regenerated, and four-wave-mixing peaks. The main peak is from the original slave laser, the regenerated peak comes from the master laser's photon, and the FWM peak is generated by the saturation-induced refractive index variation effect inside the cavity [28, 30]. From the optical spectrum, the power intensity ratio between the FWM peak and the master laser's peak can be expressed as [30]:

#208831 - $15.00 USD Received 24 Mar 2014; revised 10 May 2014; accepted 11 May 2014; published 22 May 2014

$$\left|\frac{A_f}{A_r}\right|^2 = \frac{\left(\Omega^2\gamma_p^2 + \Omega_r^4\right)\left(1+b^2\right)/4}{\left(\Omega^2 - \Omega_r^2/2 - b\Omega\gamma_p/2\right)^2 + \left(\Omega\gamma_r - \Omega\gamma_p/2 - b\Omega_r^2/2\right)^2}, \tag{2}$$

where A_f is the amplitude of the FWM field, A_r is the amplitude of the regeneratively amplified field, Ω_r is the relaxation resonant frequency, γ_p is the relaxation rate contributed by the derivative of the non-linear gain parameter, γ_r is the overall relaxation rate, and b is the linewidth enhancement ratio. The value of Ω is determined by the angular detuning frequency ($2\pi\Delta f$). From the measured RF spectrum, the output microwave power of the slave laser can be written as [30]:

$$\sigma^2 = \left|\frac{\eta A_i}{A_0}\right|^2 \frac{\Omega^2 + \left(\gamma_r - \gamma_p\right)^2}{\left(\Omega^2 - \Omega_r^2\right)^2 + \Omega^2\gamma_r^2}, \tag{3}$$

where the η is the coupling rate, A_i is the amplitude of the injection signal from the master laser, A_0 is the steady-state field intensity inside the slave laser, and the rest parameters are the same as Eq. (2). While the determination of A_i and A_0 could be easier in the experiments by using discrete modules, it is difficult for us to decide these parameters in an integrated chip. Furthermore, due to the current-dependent wavelength shift and linear output power-to-current relation in the integrated platform, the influences from the master laser is subject to a more complicated situation. If we consider a general case in which the master laser emits shorter wavelength photons and sweeps across the slave laser's peak, then the A_i is smaller at the beginning of the process ($\lambda_{master}<\lambda_{slave}$, $\Delta f>0$) than that at the end ($\lambda_{master}>\lambda_{slave}$, $\Delta f<0$). Meanwhile the variation of A_0 can be negligible to the first order. Thus the Eq. (3) is no longer symmetric to the origin of the frequency detuning and has a higher value at negative detuning branch than the positive one. Hence, the generated microwave power spectrum, σ^2, will bear asymmetric pattern once this variation of injected power is considered. To simplify our fitting calculation, we put the pre-factor term of η, A_i and A_0 into one combined fitting parameter, named the coupling coefficient, and this combined coefficient showed a traditional roll-over profile just like the L-I characteristics of the laser. The extracted parameters are listed in Table 1. The relaxation resonant frequency of 8.96 GHz is close to what an individual DFB laser with the similar structure was demonstrated before [34].

From Fig. 9, several points in (a) and (b) deviates from the theoretical calculation. The main reason is due to the strong non-linear reaction of P1 state, where the RF output is fixated at f_r and does not respond to the further current tuning of the emission wavelength. Also at close to zero detuning frequency, chaos took place and no simple pattern can be identified under the same criteria. Once the separation of the emission wavelength becomes greater, the laser is back to the FWM state and we saw a very good match between the experimental data and calculation.

From these parameter extractions, one could extend the previous calculation to estimate the possible effects on the DBR design towards the RF performance. Equation (3) can calculate the generated RF power under different coupling coefficient ($|\eta A_i/A_o|^2$), which is closely related to the number of DBR pairs. The RF tuning range can also be obtained if we assume −50dB (10dB above the noise floor) is the minimum power to receive. Figure 10 shows the combined results of such calculation based on the parameters extracted in Table 1. Three regimes of laser operations are marked in the plot. If the number of DBR pairs is larger than 4.5 (area A), the laser can operate in single mode and the calculation by Eq. (3) is valid. However, if the DBR pairs are equal or fewer than 3.5 (area C), even though the predicted tuning range and RF power can be increased significantly, the laser operates in multiple longitudinal mode, which can deteriorate the four-wave-mixing completely and invalidate the projected calculation. Between these two regions, the grey area B means the laser could be either in the single or multimode

#208831 - $15.00 USD Received 24 Mar 2014; revised 10 May 2014; accepted 11 May 2014; published 22 May 2014

and the RF behavior will be demonstrated if the laser is single-mode. So from this point of view, to have a solid microwave generator, our device must equip with at least 4.5 pairs of DBR and the RF tuning range is between 50GHz to 70GHz.

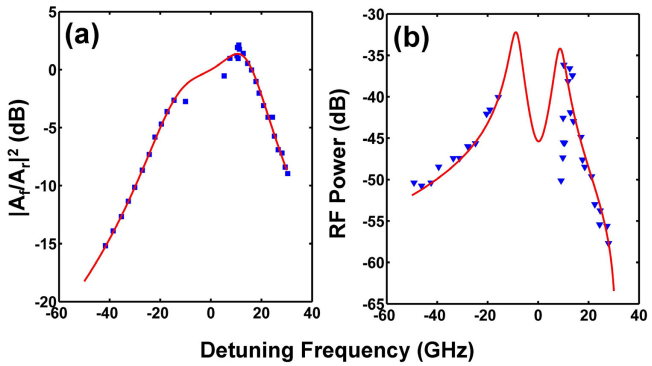

Fig. 9. The measured (blue dots) and fitted (red lines) results of (a) the power ratio of FWM and regenerative amplified peak; (b) RF power; both at the I_{slave} = 58mA, and I_{master} = 16 to 80mA. The frequency detuning is used as the variable. When the detuning diminishes towards zero, the strong chaotic behavior of the laser cause the spreading of the experimental data.

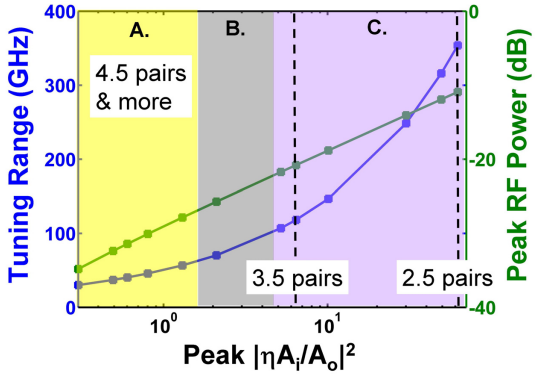

Fig. 10. The tuning range and peak RF power calculated by Eq. (3) and based on the extracted parameters in Table 1.

7. Conclusion

In summary, we demonstrated a full dynamic behavior map of a monolithic dual-wavelength DFB laser suitable for microwave generation. The nano-scale DBR structure was inserted between the two DFB lasers to create a weak coupling while maintaining single mode operation of lasers. According to different driving current combination, the RF output of the device can exhibit single mode, multiple mode or even chaos patterns. The detailed map can be a very useful tool for engineers to apply such device for microwave carrier generation. A wide and continuous range of single mode from 15GHz up to 50GHz is realized via various combinations of I_{slave} and I_{master}. A further investigation reveals the inherent laser parameters from the optical and microwave measurement of the device. The resonant frequency of 8.96 GHz and the linewidth enhancement factor of 7.7 are obtained. The single mode RF spectrum was also examined in details and the linewidth of 2.22MHz is found. We believe this kind of device can provide a small-footprint and energy-efficient choice for the future microwave systems.

#208831 - $15.00 USD Received 24 Mar 2014; revised 10 May 2014; accepted 11 May 2014; published 22 May 2014

Table 1. Parameter extraction from a dual-wavelength DFB laser

Laser Parameters	Extracted Values
The total relaxation rate (γ_r, in ns^{-1})	30.03
The relaxation rate by non-linear gain parameter (γ_p, in ns^{-1})	1.77
The relaxation resonant frequency (f_r, in GHz)	8.96
Linewidth enhancement factor (b)	7.7

Acknowledgments

Authors would like to thank Prof. H.-C. Kuo, Prof. J.-H. Chen of NCTU, Dr. Y.-J. Cheng of SINICA in Taiwan and Santur Corporation, Inc. USA for their technical supports. This work is supported by Ministry of Science and Technology of Taiwan through the contracts: NSC 102-2120-M-110-005, and NSC 101-2221-E-009-046-MY3.

#208831 - $15.00 USD Received 24 Mar 2014; revised 10 May 2014; accepted 11 May 2014; published 22 May 2014